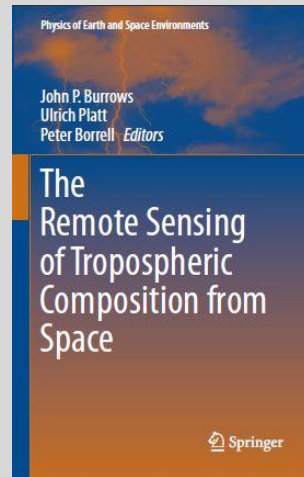


The Remote Sensing of Tropospheric Composition from Space

Editors:

John P. Burrows
Ulrich Platt
Peter Borrell

Pages 123 - 152



Chapter 3

Thermal Infrared: Absorption and Emission – Trace Gases and Parameters

Cathy Clerbaux, James R. Drummond,
Jean-Marie Flaud and Johannes Orphal

Publisher: Springer Verlag, Heidelberg

[Springer Book Web Page](#)

[Springer on line Page for the Book](#)

ISBN 978-3-642-14790-6

DOI 10.1007/978-3-642-14791-3

February 2011

Chapter 3

Using Thermal Infrared Absorption and Emission to Determine Trace Gases

Cathy Clerbaux, James R. Drummond, Jean-Marie Flaud and Johannes Orphal

3.1 Physical Principles

Thermal infrared radiation is more commonly known as radiative heat. The thermal infrared region is the wavelength range of the electromagnetic spectrum which is characteristic of the thermal or heat radiation from the Earth's surface and from the atmosphere (McCartney 1983). In thermal equilibrium, the emission of radiation in the infrared is governed by Planck's law, which describes the spectral distribution of the energy emitted by "black" bodies (i.e. having unit emissivity at all wavelengths) as a function of temperature (see Chapter 1). Both the Earth's surface and the atmosphere emit in the so-called "thermal" infrared, having spectral distributions described by the Planck function corresponding to the local temperature, i.e. the surface temperature of the Earth and the temperature as function of altitude. However, it is important to note that neither the Earth's surface nor the atmosphere are perfect black bodies, so that a correction factor – the "emissivity" which is wavelength-dependent – needs to be used. As the temperature of the Earth's surface is about 300 K (see Fig. 3.1), from Planck's law the maximum of the thermal emission is predicted at a wavelength of around 10 μm (wavenumber: 1,000 cm^{-1}).

Thermal infrared corresponds to the wavelength region from about 3 μm to 100 μm (about 100–3,000 cm^{-1}), but there is actually no strict limit, in particular at longer wavelengths. The Earth's thermal emission is present during day and night which is important for atmospheric remote-sensing applications. Thermal infrared

C. Clerbaux (✉)

UPMC Univ. Paris 06; CNRS/INSU, LATMOS-IPSL, Paris, France

J.R. Drummond

Department of Physics and Atmospheric Science, Dalhousie University, Halifax, Canada

J.-M. Flaud

Université Créteil Paris 12, CNRS UMR 7583, LISA-IPSL, Paris, France

J. Orphal

Institute for Meteorology and Climate Research (IMK), KIT, Karlsruhe, Germany

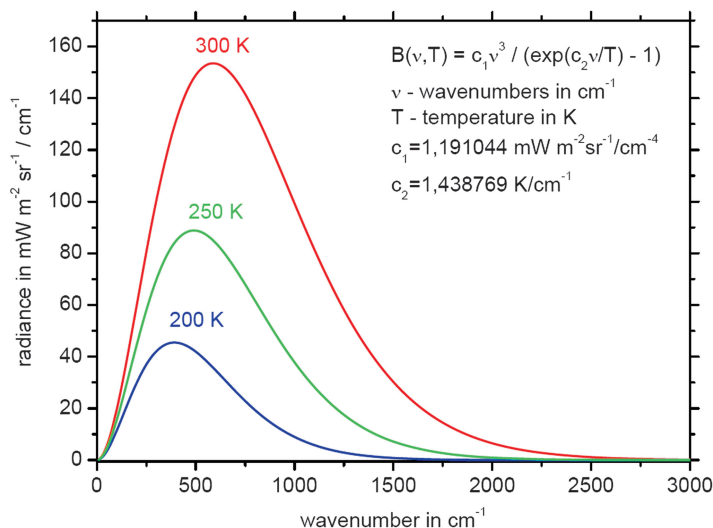


Fig. 3.1 Thermal emission in the infrared as function of temperature, described by Planck's law. Curves for typical atmospheric temperatures are shown. Note the increase of the emitted energy as function of temperature that scales with T^4 (Stefan-Boltzmann law) and the shift of the maximum of the emission to longer wavelengths when the temperature decreases (Wien's law).

is also a part of the solar spectrum and can thus be exploited for satellite measurements that operate in solar occultation mode.

Most atmospheric constituents absorb and re-emit infrared photons, but the strongest spectral features are due to rotational-vibrational transitions allowed by the quantum mechanical selection rules. In particular transitions that lead to a change of the molecular dipole moment upon absorption or emission of a photon are allowed. Homo-nuclear diatomic molecules like N_2 or O_2 therefore do not show strong spectral features in the thermal infrared which is an advantage for remote-sensing since the atmosphere is then largely transparent in this spectral region. However hetero-nuclear diatomic molecules (such as CO , NO , HF , HCl , etc.) and also most polyatomic molecules (like H_2O , CO_2 , N_2O , CH_4 , NO_2 , HNO_3 , OCS , SO_2 , etc.) show strong absorption and emission in the thermal infrared. In addition, higher-order effects exist such as pressure-induced absorption or emission (that are especially important for N_2 , O_2 , and CO_2) and radiative effects beyond the wings of spectral lines (the so-called "continua" of N_2 , O_2 , and H_2O), that have to be included in numerical models of the radiative transfer in the Earth's atmosphere. Thus, the emission spectrum of the Earth's atmosphere contains many spectral features due to the different molecules that absorb and emit radiation (see Fig. 3.2); furthermore, due to the highly variable vertical temperature profile in the atmosphere, the observed spectrum is a superposition of all these processes at different altitudes, so that radiative transfer models are required to calculate (and analyse) infrared atmospheric spectra (see also Chapters 1 and 4).

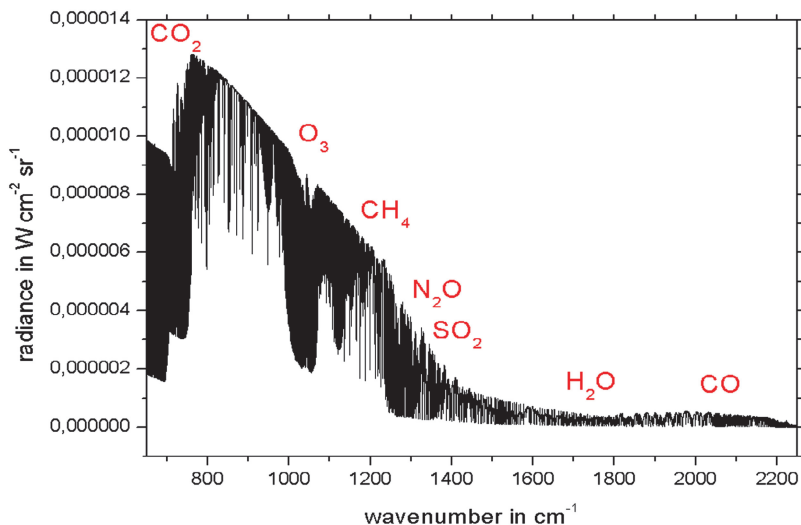


Fig. 3.2 The thermal emission of the Earth's atmosphere in the infrared (nadir geometry) for standard conditions, calculated at high spectral resolution with a radiative transfer model (Orphal et al. 2005). The envelope is given by the Planck function corresponding to the surface temperature (about 300 K) but one can see the strong absorptions due to water vapour, CO₂ and O₃. The radiance below the strongest bands of O₃ (around 1,000 cm⁻¹) and CO₂ (around 650 cm⁻¹) does not fall to zero since these molecules also re-emit radiation corresponding to the Planck curves of their respective temperatures (see Fig. 3.1).

Each molecule possesses a characteristic absorption (and emission) spectrum in the thermal infrared that needs to be measured first in the laboratory. Furthermore, in order to predict the variation of the molecular spectra as a function of temperature, it is essential to know the exact energy of the rotational-vibrational energy levels that are involved in the infrared transition (absorption or emission). For this purpose, quantum mechanical calculations are performed that provide these energy levels as a function of the vibrational and rotational quantum numbers, using theoretical models that take into account different rotation-vibration interactions for each molecule: diatomic or linear molecules (including degenerate modes), symmetric, asymmetric or spherical tops, spin-rotation interactions for radicals, and also large amplitude motions for “floppy” molecules like H₂O or NH₃. It is important to stress that the measurement and theoretical analysis of molecular spectra are a considerable ongoing effort, since they are essential for the understanding and numerical modelling of atmospheric spectra.

An important effect – only visible at relatively high spectral resolution – is the broadening of the individual molecular lines when the total pressure increases; in the Earth's atmosphere this effect leads to a Lorentz profile with molecular linewidths of about 0.2–0.4 cm⁻¹ (full width at half maximum, at one atmosphere total pressure). The exact magnitude of this effect depends on the molecule and rotational quantum numbers, and again, laboratory measurements and theoretical models are needed to determine the pressure broadening parameters. The intrinsic line broadening due to

the thermal Doppler effect is usually small in the mid-IR spectral region (Chapter 1). Although the “standard” line profile in the thermal infrared is a Voigt profile (a convolution of the Lorentz profile due to the pressure broadening with the Gaussian profile due to the thermal Doppler effect), small deviations from the Voigt profile (so-called “collisional narrowing” effects) have been observed in the laboratory and in atmospheric spectra, and need to be taken into account in the analysis of high-resolution atmospheric spectra. More interestingly, the pressure broadening effect can provide further, independent information for the vertical concentration profiles of atmospheric trace gases, in addition to the observational geometry (see below) and to the variation of the molecular spectra as a function of temperature. An even smaller effect – that is however also important at high spectral resolution – is the shift of the line centre as a function of total pressure (typically a few 0.001 cm^{-1} per atmosphere).

Molecular line parameters (line positions, line intensities, lower state’s energies, pressure broadening and pressure shift parameters) are available from spectroscopic databases such as HITRAN (Rothman et al. 2005; 2009) or GEISA (Jacquinet-Husson et al. 2008) that are updated on a regular basis. These databases also contain some parameters for aerosols (refractive indices) and absorption cross-sections for molecules with very dense spectra that are not easily resolved into individual lines (e.g. the CFCs, N_2O_5 and ClONO_2). Note that for some remote-sensing experiments like ATMOS, MIPAS or IASI (see below), dedicated spectroscopic databases have been prepared containing reference data that cover only the spectral region and molecules of interest.

For numeric modelling of thermal infrared radiation, many computer codes are available but they always need to be adapted to the detailed purposes of the remote-sensing application. In particular, it is important to stress that the radiative transfer modelling of atmospheric spectra in the thermal infrared is a very challenging task, that can take up to several minutes – even on very modern computers – for a broad spectral region (e.g. some 100 cm^{-1}) at high spectral resolution (e.g. 0.001 cm^{-1}). This is especially important for the inverse problem where concentration profiles of atmospheric trace gases are determined from spectra in the thermal infrared (see below) and many radiative transfer calculations are required for each retrieved profile. It is also important to note that vertical profiles of temperature and pressure are always required for radiative transfer modeling in the thermal infrared, and some other auxiliary parameters, such as the surface temperature and emissivity, the aerosol content, and cloud parameters (e.g. cloud coverage, cloud height, cloud temperature) are also needed. Some information on these parameters can, in principle, also be extracted from the infrared spectra themselves, but this may lead to significant correlations between the retrieved atmospheric parameters.

Finally, there are several intrinsic advantages when using the thermal infrared region for atmospheric remote sensing.

- Many molecules that are observed in the thermal infrared cannot be measured in other spectral regions.
- Since the processes of absorption and emission of infrared photons are governed by Planck’s law, they are very sensitive to temperature, as are the molecular line

strengths (due to the temperature-dependent population of the molecular energy levels), and this leads to vertical information that can be extracted from atmospheric spectra in the thermal infrared – even when using nadir (down-looking) geometry from space.

- The pressure-dependence of the molecular line-widths provides additional vertical information, although a high spectral resolution is required to observe this effect.
- Observations in the thermal infrared can be made both day and night, so that – in contrast to remote-sensing measurements in the ultraviolet-visible spectral region – diurnal cycles can be observed, as can species that are only present in significant concentrations during the night.

3.2 Thermal Infrared Instruments: Techniques, History, Specificity

3.2.1 Techniques

Remote sensors using the thermal infrared spectral range use different instrumental design, depending on their primary mission goal. Past and current instruments are based on evolving technology such as cell correlation radiometry, Fourier transform spectroscopy, or grating spectrometry.

a Cell Correlation Radiometry

A correlation cell radiometer (also called gas correlation sensor) forms an optical filter specific to the gas being monitored by passing the optical signal through a cell of the same gas within the instrument. The amount of gas (i.e. its density) is varied by varying length or pressure within the cell. The change in signal is greatest near the spectral lines of the gas being investigated, and between the spectral lines both the cell absorption and the change in absorption with the quantity is minimal. The instrument has good selectivity (effective spectral resolution) due to the close association of the change of signal with the spectral lines themselves, good signal-to-noise ratio because many lines are monitored simultaneously, and a modest data rate because only one optical signal is detected.

b Fourier Transform Spectroscopy

Fourier transform infrared spectroscopy (FTS) is a measurement technique for collecting infrared spectra using a Michelson-type interferometer. The thermal infrared radiation emitted from the Earth-Atmosphere system (i.e. the source of

photons) is split into two beams by a half-transparent mirror called a beam-splitter, one is reflected from a fixed mirror and one from a moving mirror, which introduces a time delay, or optical path difference. The two beams are then allowed to interfere, and the overall intensity of the light is measured at different time delay settings. By making measurements of the signal at many discrete positions of the moving mirror (the so-called “interferograms”), the source spectrum can finally be reconstructed using the inverse Fourier transform. In order to avoid oscillations around spectral lines that are due to the finite length of the interferograms, the latter are usually multiplied by a numerical function that decreases to zero at maximum delay; this operation is called “apodisation” and slightly reduces the spectral resolution.

c Grating Spectrometry

A grating spectrometer disperses light incident on it, i.e. a spectrum of radiation is separated in space by wavelength, using a prism or a grating. The dispersed light is then recorded by a focal plane detector array (an arrangement of many small detectors in a line, for example, on a semiconductor chip). Multi-aperture array grating spectrometers are used in space and provide high spectral resolution with wide spectral coverage, using advanced imaging design, with wide spectral coverage. Note that both interferometers and grating spectrometers make use of the interference of electromagnetic radiation.

Upwelling radiance enters the system via the cross-track scan mirror, where it is directed into a telescope. The collimated energy exiting the telescope is incident on the spectrometer entrance slit plane containing individual apertures. Ultimately, these slits are imaged onto the focal plane, where each slit image contains the energy from one selected grating order.

3.2.2 History

As satellite technology improved in the late twentieth century, it became possible to expand the range of wavelengths measured from space and to increase the spectral resolution available. Both of these are essential to successful measurements of atmospheric composition. The first instruments were targeted at the middle atmosphere to measure stratospheric ozone and related species (e.g. the UARS mission launched in 1991) and the tropospheric capability was an incidental ability. However substantial progress was made with a number of instruments.

The Atmospheric Trace Molecule Spectroscopy (ATMOS) Experiment (Gunson et al. 1996) was flown by NASA on the space shuttle on four occasions in 1985, 1992, 1993 and 1994. It consisted of a Fourier transform spectrometer with a sun-tracker and measured the atmosphere twice per orbit, by solar occultation at sunrise and sunset. Its spectral resolution was 0.01 cm^{-1} (unapodized) in the wavelength

range $600\text{--}4,800\text{ cm}^{-1}$, although this range was accomplished in a number of separated spectral intervals (channels), rather than a continuous scan.

The Measurements of Atmospheric Pollution from Satellites (MAPS) instrument (Reichle et al. 1999) was also a shuttle instrument, but was targeted specifically at CO in the troposphere. It flew on the shuttle in 1981, 1984 and 1994. The instrument was a fixed-cell correlation radiometer operating in the $4.7\text{ }\mu\text{m}$ region of the fundamental band of CO. The instrument viewed downwards – nadir– and therefore had good horizontal resolution, but poor vertical resolution. MAPS produced the first directly measured maps of a tropospheric minor constituent (apart from water vapour). MAPS showed the importance of tropospheric monitoring from space by demonstrating the significant temporal and spatial variation in constituents. It also illustrated the problems of cloud cover for such instruments and the issues of coverage during a limited-duration mission.

The Interferometric Monitor for Greenhouse Gases (IMG) (Kobayashi et al. 1999) was the first satellite-borne instrument launched to use the thermal infrared spectral range to sound the troposphere. It was carried on the ADEOS-1 platform, and provided 10 months of data, from August 1996 to June 1997, until the failure of the platform solar array. IMG was a nadir-looking Fourier transform spectrometer which recorded the thermal emission of Earth between $600\text{ and }3,030\text{ cm}^{-1}$, with a spectral resolution of $\sim 0.1\text{ cm}^{-1}$. Owing to the polar orbit of the ADEOS satellite, IMG allowed the simultaneous measurement and global distributions from space for a series of trace gases relevant for climate and chemistry studies: H_2O , CO_2 , N_2O , CH_4 , O_3 , CO, CFCs, and HNO_3 (Clerbaux et al. 2003). For some species, the high spectral resolution allowed vertical profiles to be derived.

3.2.3 *Specificity*

When using the thermal infrared spectral range to sound the atmosphere, a remote sensor on board a satellite records the light passing through different atmospheric layers. From the radiance signal recorded, one can extract information on the vertical concentration of each atmospheric constituent absorbing at a given altitude. The source can be either the thermal emission of the Earth-atmosphere system (nadir and limb viewing, Section 3.1 and Chapter 1), or a section of the solar emission spectra (solar occultation). Solar occultation or limb-viewing instruments provides extremely high sensitivity to trace constituents due to the long atmospheric paths and the strength of the solar source (equivalent to a blackbody at about $5,800\text{--}6,000\text{ K}$). It also provides excellent vertical resolution, but poor horizontal resolution, each due to the path geometry in the atmosphere. Solar occultation works well in the middle and upper atmosphere where general transparency is high, but runs into difficulty when clouds and heavy aerosol layers, or strong absorbers such as water vapour, are present in the path, as occurs in the troposphere. Therefore as the tangent height – the height of the lowest point on the light path – decreases, the frequency of useful measurements declines.

For cloud free situations, nadir-looking thermal infrared instruments can measure the atmospheric radiation down to the ground and some vertical information can be derived from the shape of the absorption lines, provided the spectral resolution is high enough. The thermal contrast between the surface and the boundary layer determines to what extent one can detect species near the surface. The Earth's surface either heats up or cools down faster than the atmosphere and, therefore, the diurnal variation is larger, and hence thermal contrast more pronounced during day than night. The capability of an infrared nadir sounder to probe the lower atmospheric layers, where local pollution occurs, therefore strongly depends on location, the temperature, the type of surface (emissivity) and the time of the day. Thermal contrasts are generally highest over land during the day and lowest over water at night. This, along with the instrumental characteristics (spectral resolution and radiometric noise) determines the amount of vertical information that can be retrieved for a given species in the nadir geometry, and the uneven sensitivity to the atmospheric layers (averaging kernels, see Section c below).

a Retrieval Algorithms/Inversions

Inversion of geophysical parameters from remotely sensed observations is known to be an ill-posed problem (Rodgers 1976). A variety of methods exist for the retrieval of atmospheric profiles from the spectra measured by remote sounders. A large body of literature is available on the subject, and the most widely used approaches in atmospheric remote sensing are described, for example, in Rodgers (2000) and Tarantola (2005). The accuracy of the retrieved quantities and the ability to retrieve low-resolution vertical profiles from the data provided by an instrument partly rely on the efficiency of the inversion procedure.

b Forward Radiative Transfer

Given the general radiative transfer equation, the measurement \mathbf{y} can be expressed as the vector of measured quantities (radiances):

$$\mathbf{y} = \mathbf{F}(\mathbf{x}, \mathbf{b}) + \boldsymbol{\epsilon} \quad (3.1)$$

where \mathbf{F} is the forward radiative transfer function, \mathbf{x} denotes the vector of atmospheric states, for example, the trace gas concentration at different altitudes, \mathbf{b} represents model parameters affecting the measurement and $\boldsymbol{\epsilon}$ is the measurement noise. As described in Section 3.1, a synthetic spectrum can be computed using the line parameters (positions, intensities, broadening and shifting parameters, including their dependence on temperature), and absorption cross sections for the heavier molecules, as collected in spectroscopic databases such as HITRAN and GEISA (Rothman et al. 2005; Rothman et al. 2009; Jacquinet-Husson et al. 2008).

The water vapour, CO₂, O₂ and N₂ continua also have to be included to represent the atmosphere correctly. The resulting spectrum should then be processed to take into account the Instrumental Line Shape (ILS).

Useful variables are the derivatives of the radiance with respect to the parameters to retrieve, the Jacobians $\mathbf{K} = \partial\mathbf{y}/\partial\mathbf{x}$ (\mathbf{x} includes the vertical abundances of the target species), as well as to the model parameters $\mathbf{K}_b = \partial\mathbf{y}/\partial\mathbf{b}$.

c The Optimal Estimation (OE) Formalism

i Finding an Optimal Solution

Starting from relevant *a priori* information, composed of a mean state \mathbf{x}_a , and an *a priori* covariance matrix, \mathbf{S}_a , which represents the best statistical knowledge of the state prior to the measurements, the retrieved state can then be found using the Optimal Estimation Method. Assuming a linear problem, the optimal vertical profile can be written as (Rodgers 2000):

$$\hat{\mathbf{x}} = (\mathbf{K}^T \mathbf{S}_e^{-1} \mathbf{K} + \mathbf{S}_a^{-1})^{-1} (\mathbf{K}^T \mathbf{S}_e^{-1} \mathbf{y} + \mathbf{S}_a^{-1} \mathbf{x}_a) \quad (3.2)$$

where \mathbf{S}_e is the measurement covariance matrix

Introducing the gain and averaging kernels matrices \mathbf{G} and \mathbf{A} ,

$$\mathbf{G} = \frac{\partial \hat{\mathbf{x}}}{\partial \mathbf{y}} = (\mathbf{K}^T \mathbf{S}_e^{-1} \mathbf{K} + \mathbf{S}_a^{-1})^{-1} \mathbf{K}^T \mathbf{S}_e^{-1} \quad (3.3)$$

$$\mathbf{A} = \frac{\partial \hat{\mathbf{x}}}{\partial \mathbf{x}} = \mathbf{G} \mathbf{K} \quad (3.4)$$

Eq. 3.2 can also be rewritten as:

$$\hat{\mathbf{x}} = \mathbf{x}_a + \mathbf{A}(\mathbf{x} - \mathbf{x}_a) + \mathbf{G}(\boldsymbol{\varepsilon} + \mathbf{K}_b(\mathbf{b} - \hat{\mathbf{b}})) \quad (3.5)$$

ii Information Content

The element $\mathbf{A}(i,j)$ of the averaging kernel matrix \mathbf{A} is the relative contribution of the element $\mathbf{x}(j)$ of the true state to the element $\hat{\mathbf{x}}(i)$ of the retrieved state. The vertical resolution of the retrieved profile can be defined as the full width at half maximum of the rows of the averaging kernel matrix. The number of independent elements of information contained in the measurement can also be estimated as the Degrees Of Freedom for Signal (DOFS) which is defined as the trace of the averaging kernel matrix (Rodgers 2000). Examples of typical averaging kernel functions for nadir looking thermal infrared instruments are provided in Fig. 3.3.

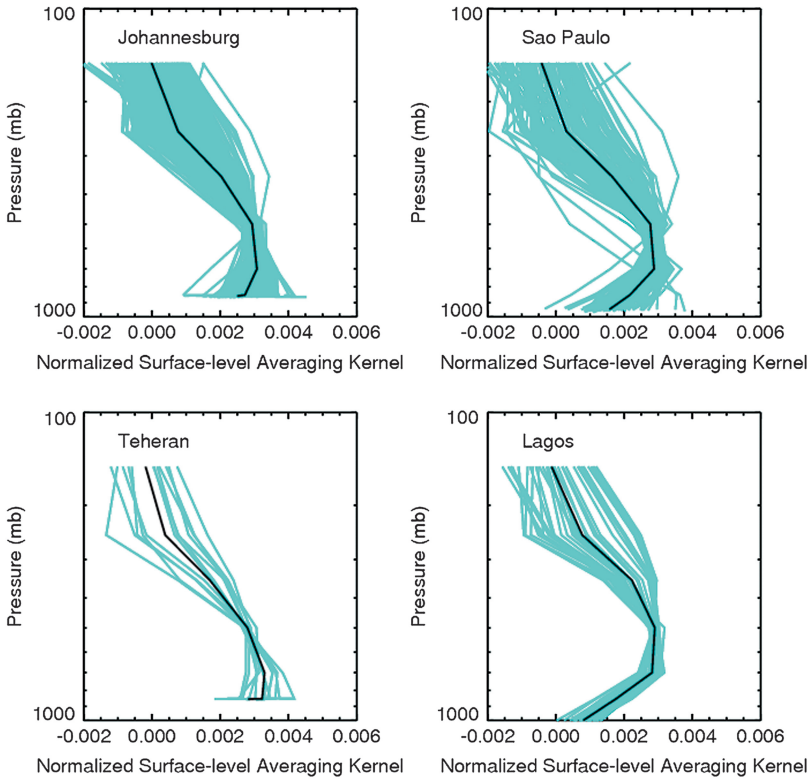


Fig. 3.3 Surface level averaging kernels above Johannesburg (South Africa), Teheran (Iran), Sao Paulo (Brazil) and Lagos (Nigeria) as observed by MOPITT in 2004. The *blue lines* correspond to single observations and the *black line* is an average over all observations (adapted from Clerbaux et al. (2008a)).

iii Error Budget

In the linear approximation, the total error is computed from the linear retrieval equation (Eq. 3.5) as the difference between the true state and the retrieved state:

$$\hat{\mathbf{x}} - \mathbf{x} = (\mathbf{A} - \mathbf{I})(\mathbf{x} - \mathbf{x}_a) + \mathbf{GK}(\mathbf{b} - \hat{\mathbf{b}}) + \mathbf{G}\boldsymbol{\varepsilon} \quad (3.6)$$

where \mathbf{I} is the identity matrix. This equation illustrates the three principal sources of error.

1. The smoothing error, $(\mathbf{A} - \mathbf{I})(\mathbf{x} - \mathbf{x}_a)$, which accounts for the smoothing of the true state by the averaging kernels.

2. The model parameters error, $\mathbf{GK}(\mathbf{b} - \hat{\mathbf{b}})$ which accounts for the imperfect knowledge of the direct model parameters.
3. The measurement error, $\mathbf{G}\varepsilon$, associated with the radiometric noise.

d The Tikhonov–Philips Regularization

A modification of the optimal estimation (OE) formalism is the so-called Tikhonov–Philips (TP) regularization. Here, instead of the *a priori* covariance matrix, \mathbf{S}_a , which has to represent the best statistical knowledge of the state prior to the measurements, a regularization matrix \mathbf{R} is used to constrain the solution. The method is used, for example, when no precise *a priori* covariance matrix is available, or when the constraint of the retrieval needs to be optimized for a particular vertical region, or for the vertical smoothness of the solution, e.g. for retrievals from limb geometry (Steck 2002). Whereas the strength of the constraint in the “classical” regularization method (Tikhonov 1963; Phillips 2003) is the same for all the altitudes, it may be dependent of the altitude for particular atmospheric retrieval methods (Doicu et al. 2004; Kulawik et al. 2006).

Mathematically, this means that the inverse of matrix \mathbf{S}_a in Eq. 3.3 is replaced by the matrix \mathbf{R} so that the entire retrieval formalism and software codes are the same for both the OE and TP methods. In particular, diagnostic variables like DOFS, are also used for the TP regularization method, and the calculation of the error budget and vertical resolution (using the averaging kernel matrix \mathbf{A}) is also essentially the same. The TP method has been applied to the analysis of spectra obtained with several limb and nadir looking sounders (Fischer et al. 2008; Keim et al. 2008; Kulawik et al. 2006; Bowman et al. 2006; Worden et al. 2007a; Eremenko et al. 2008).

The question of which method (OE or TP) is to be used for a particular retrieval problem is difficult to answer since there is no general recipe for defining the “best” covariance (\mathbf{S}_a) or regularization (\mathbf{R}) matrices. The OE method will always provide the “optimum” solution that is statistically the most probable (based on the existing data that are represented by the *a priori* covariance matrix \mathbf{S}_a), while the TP method may be interesting for situations where such a matrix is difficult to define, here great care has to be taken to construct regularization matrices that provide physically meaningful results, in particular to avoid excessive or too weak constraints.

e Neural Networks

Statistical methods using neural networks (Fig. 3.4) offer interesting possibilities for solving problems involving complex transfer functions in a time efficient manner. The first step building an efficient neural network is to define its architecture. In the literature, multilayer networks are shown to provide good performance

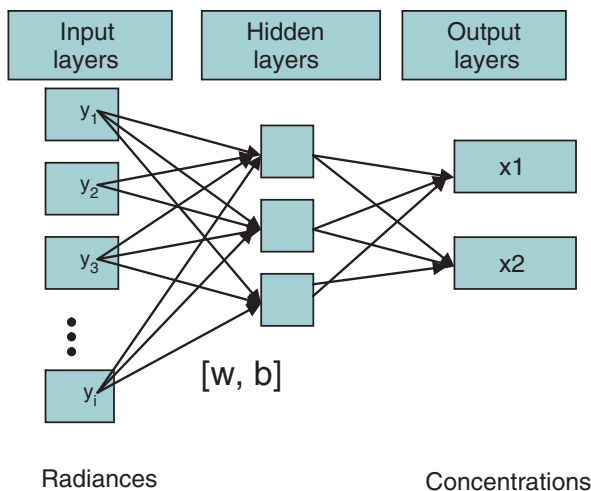


Fig. 3.4 Schematic representation of a neural network, including inputs (recorded radiances), hidden layers with mathematical functions, and outputs (concentrations of trace gases).

in solving problems with geophysical variables. To characterize the architecture of this type of neural network, the number of layers and of neurons. Each neuron is a mathematical function in each layer, and the topology of their connections, must be carefully chosen, as well as the transfer functions used. This is done on the basis of empirical considerations which depend on the complexity of the function associated with the physical problem to solve.

Once the architecture is fixed, the training begins by fitting the parameters of the neural model: weights of the connections and bias associated with neurons. For trace gas retrieval, this training phase consists in associating the input radiance measurement vector (\mathbf{y}) with the desired column or profile concentration output (\mathbf{x}). This is done by modifying the parameter weights and bias values, using for example a gradient back-propagation algorithm. In order to build a comprehensive database to train the network, atmospheric concentration profiles, either provided by chemical-transport models, or from independent observations, are used as input to a line-by-line radiative transfer code, and then the spectra are convolved with the instrumental function. The weights and bias are first initialized to random values. Then the square of the differences between the desired and the calculated outputs (trace gas concentration) for the whole the training dataset is minimized through an iterative gradient descent procedure, and the parameters matrix is modified accordingly. This requires a long computation time because of the minimization process. Once the network is trained, the weights and biases are held fixed and the network is ready to operate. This retrieval technique is particularly useful in case of very high data rates and/or time constraints (e.g. if operational retrievals are needed) as it is very efficient in time (Turquety et al. 2004).

3.3 Thermal Infrared: Missions and Products

Information on all the satellite-borne missions using thermal infrared that flew or are still operating now is included in Appendix A.

In the thermal infrared spectral range, most of the key atmospheric species exhibit significant absorptions provided they are present in the atmosphere with sufficient concentrations, which is directly related to their source strength and atmospheric lifetime. Table 3.1 summarises the spectroscopic absorptions of the common species. Figs. 3.5 and 3.6 are illustrations of atmospheric spectra recorded by MIPAS/ENVISAT (limb sounding geometry) and IASI/METOP (nadir looking geometry), together with the identification of the main absorbing molecules, as a function of wavenumber.

3.4 Examples

This section provides some highlights of specific results obtained from thermal infrared remote sensors, both in the limb and nadir-looking modes.

3.4.1 *Limb and Solar Occultation Instruments*

a ACE-FTS

The Atmospheric Chemistry Experiment mission (ACE, see Appendix A) was launched by CSA (Canada) on SCISAT in August 2003. ACE-FTS is a high resolution (0.02 cm^{-1}) infrared Fourier transform spectrometer operating from 2 to $13\text{ }\mu\text{m}$ ($750\text{--}4,100\text{ cm}^{-1}$) that measures the vertical distribution of trace gases and temperature using solar occultation (Bernath et al. 2005). The principal purpose of the ACE-FTS mission is to investigate the chemical and dynamical processes that control the distribution of ozone in the stratosphere and upper troposphere (10–50 km altitude range) with a particular focus on the Arctic winter stratosphere. The ACE concept is similar in some respects to the NASA ATMOS experiment that flew four times on the space shuttle between 1985 and 1994.

A 74° -inclined circular orbit with an altitude of 650 km was chosen for ACE to achieve both global and high latitude coverage. While in orbit, SCISAT observes 15 sunrises and 15 sunsets per day. During sunrise and sunset, the FTS measures infrared absorption signals that contain information about different atmospheric layers; it thus provides vertical profiles of atmospheric constituents. The vertical resolution is about 3–4 km from the cloud tops up to about 100 km. ACE measures O_3 and determines budgets for the H, N, Cl and F families of molecules. Its

Table 3.1 Molecules absorbing in the thermal infrared spectral range, with the location of absorption bands and the associated vibrational modes

Molecules	Band center (cm ⁻¹)	Absorption band (cm ⁻¹)	Vibrational mode
O ₃	710	550–900	ν_2
	1,043	919–1,243	ν_3
	1,070	940–1,280	ν_1
	2,105	1,880–2,320	$2\nu_1, 2\nu_3, \nu_1 + \nu_3$
	2,800	2,680–2,820	$\nu_1 + \nu_2 + \nu_3$
CO	2,100	2,000–2,260	1–0
SO ₂	1,151	1,080–1,260	ν_1
	1,361	1,310–1,400	ν_3
	2,499	2,440–2,530	$\nu_1 + \nu_3$
H ₂ CO	1,746	1,650 to >1,830	ν_2
	2,780–2,874	2,700 to >3,000	ν_1, ν_5
NO ₂	648	650–880	ν_2
	1,621	1,550–1,760	ν_3
	2,910	2,850–2,940	$\nu_1 + \nu_3$
PAN	–	750–1,900	Cross sections
H ₂ O	1,595	<600 to >3,000	ν_2
CO ₂	618.1		$2\nu_2(l_0)$
	667.3	<600–850	$\nu_2(l_1)$
	720.5		ν_1
	1,886	1,870–1,990	$4\nu_2(l_0)$
	2,094	2,000–2,150	$\nu_1 + 2\nu_2(l_0)$
	2,137	2,000–2,150	$2 \nu_1$
	2,349	2,000–2,700	ν_3
CH ₄	1,306.2	900–1,970	ν_4
	3,020.3	2,000 to >3,000	ν_3
CFC-11	850	810–880	ν_4
	1,082	1,050–1,120	ν_1
CFC-12	922	850–950	ν_6
	1,160	1,050–1,200	ν_8
N ₂ O	1,285	1,210–1,340	ν_1
	2,222	2,120–2,270	ν_3
HNO ₃	648.8	615–678	ν_6
	763.2	722–810	ν_8
	879.11	816–960	ν_5
	896.85	816–960	ν_9
	1,205.7	1,165–1,233	$\nu_8 + \nu_9$
	1,303.5	1,098–1,388	ν_4
	1,325.7	1,098–1,388	ν_3
	1,709.57	1,650–1,770	ν_2
	NH ₃	931(s)–967(a)	750–1,200
C ₂ H ₄	945.45	815–1,170	$\nu_7 (\nu_4, \nu_{10})$
CH ₃ OH	1,033	966–1,185	ν_8
HCOOH	1,105	960–1,235	ν_6

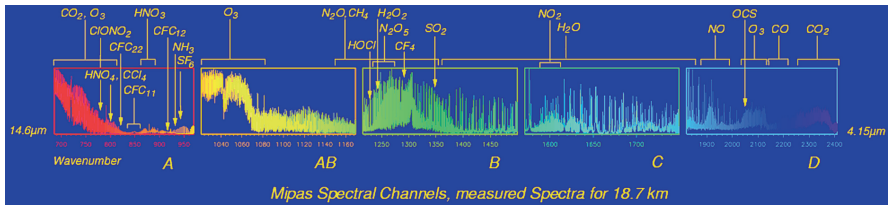


Fig. 3.5 The various spectral bands recorded by MIPAS/ENVISAT at a tangent altitude of about 19 km. The emission domains of a number of minor atmospheric constituents are indicated (Flaud and Oelhaf 2004).

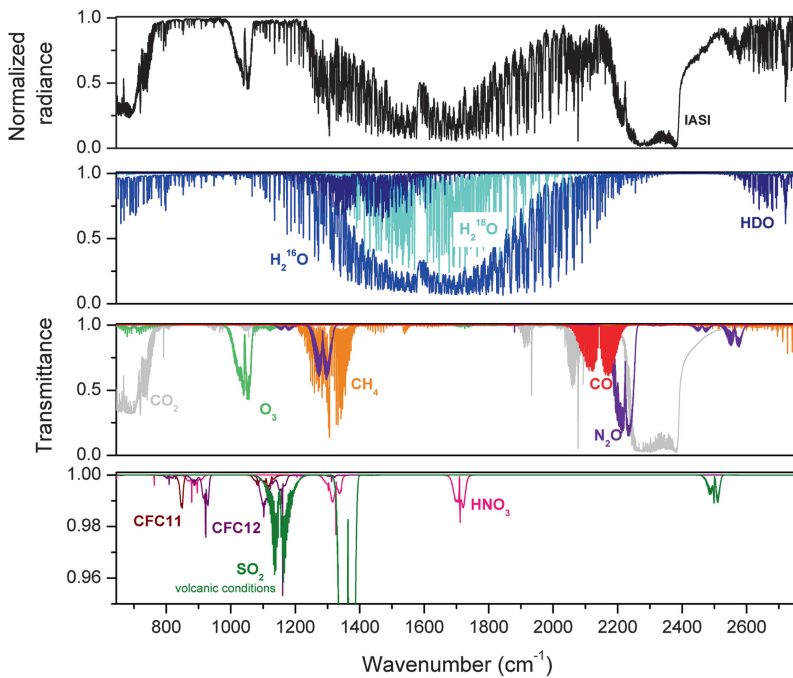


Fig. 3.6 *Top panel:* radiance atmospheric spectrum (in normalized units) recorded by IASI/MetOp, west of Australia, on 20th December 20, 2006. *Middle panels:* Nadir-looking radiative transfer simulations to identify of the main absorbing gases; *Lower panel:* and the weaker absorbers (Clerbaux et al. 2009).

capability to sound the upper-troposphere/lower stratosphere was exploited by several authors (Rinsland et al. 2006; Dufour et al. 2007; Coheur et al. 2007), see Fig. 3.7 for an illustration of the seasonal variation of CO at 16.5 km.

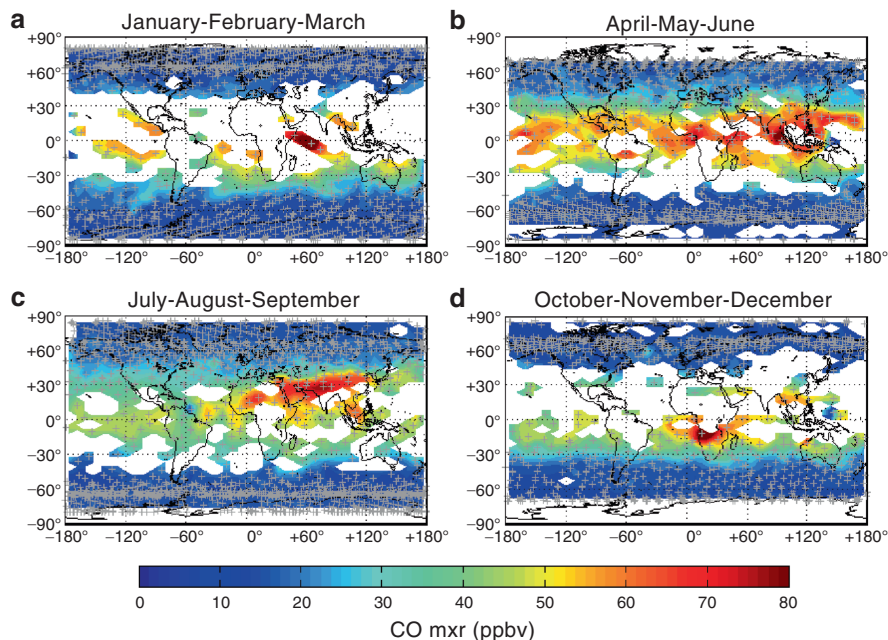


Fig. 3.7 ACE-FTS CO seasonal measurements in 2005 at 16.5 km. The data are interpolated to a 4° latitude \times 8° longitude grid. The grey crosses indicate the ACE-FTS measurement locations. Note that the tropical latitudes are not well covered in Jan-Feb-March and Oct-Nov-Dec as the satellite orbit was optimized to study the polar regions in winter (Clerbaux et al. 2008b).

b MIPAS

The Michelson Interferometer for Passive Atmospheric Sounding instrument (MIPAS, see Appendix A) was launched by ESA on ENVISAT into a polar sun-synchronous orbit in March 2002. MIPAS is a Fourier transform infrared spectrometer (Fischer et al. 2008) for the detection of limb emission spectra in the middle and upper atmosphere. It observes a wide spectral range ($4.15\text{--}14.6\ \mu\text{m}$, $685\text{--}2,410\ \text{cm}^{-1}$) with high spectral resolution ($0.025\ \text{cm}^{-1}$ unapodized). The primary geophysical parameters of interest are vertical profiles of atmospheric pressure, temperature, and volume mixing ratios of at least 25 trace constituents.

MIPAS observes the emitted radiance from the atmosphere in the limb, i.e. it is most sensitive to the atmospheric signal emitted from the tangent altitude layer and, when a limb sequence with a discrete set of different tangent altitudes is acquired, and it allows the determination of the vertical profiles of atmospheric parameters. MIPAS can measure atmospheric parameters in the altitude range from 5 to 160 km with vertical steps size between 1 and 8 km, respectively. A detailed description of the calibration and characterization of the instrument is given by Kleinert et al. (2007).

The operational MIPAS data processing by ESA generates global distributions of temperature and six key species (O_3 , H_2O , CH_4 , N_2O , NO_2 , HNO_3) while

scientific data processing has already proven that many more trace gases can be derived from the mid-infrared spectra (NO , N_2O_5 , HNO_4 , ClONO_2 , chlorine monoxide, ClO , HOCl , BrONO_2 , H_2CO , CO , CFCs, NH_3 , OCS , SO_2 , SF_6 , PAN, HCN , C_2H_6 , C_2H_2 , H_2O_2 , HDO , and O_3 iso-topologues). Furthermore, the MIPAS broadband spectra have been used for the measurement of aerosols and cloud particles (PSCs, cirrus).

Many interesting results have already been achieved from MIPAS measurements (Fig. 3.8). They include contributions to a better understanding of atmospheric processes such as pollution of the upper troposphere, troposphere-stratosphere exchange, chemistry and dynamics of the stratosphere, stratospheric ozone depletion, down-ward transport from the mesosphere into the stratosphere, interaction between varying solar radiation and atmospheric composition, and non-LTE (Local Thermal Equilibrium) effects.

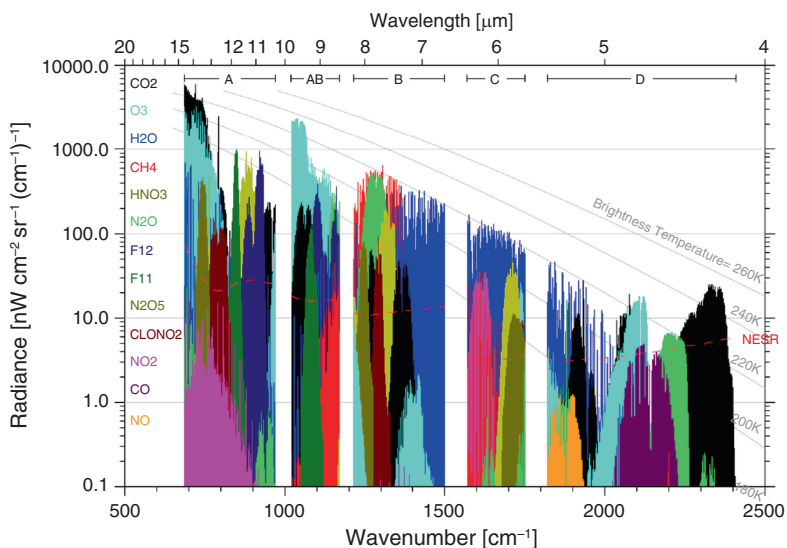


Fig. 3.8 Overview of the spectral coverage and most significant molecules covered by the five channels (A, AB, B, C, and D) of the MIPAS instrument on board ENVISAT (limb geometry, synthetic spectrum calculated for a tangent height of 12 km). Also shown are the emission curves (grey curves) corresponding to blackbody radiation at temperatures in the 180–260 K range. The dashed red line indicates the noise level (Noise-Equivalent Spectral Radiance NESR) of MIPAS for one single spectrum (Fischer et al. 2008).

Due to problems with the constant movement of the retro-reflectors of the interferometer, the measurements of MIPAS have been performed with reduced spectral resolution and a reduced duty cycle since the beginning of 2005. The spectral resolution has been reduced to 40% which in turn allows for a higher spatial resolution (vertically and horizontally). The duty cycle was further reduced later to about 35%. Nevertheless, MIPAS has detected in this mode more than 500 profiles of various atmospheric parameters, on average, every day. More

recently it was found that the problems with the moving retro-reflectors are decreasing, and therefore the duty cycle has been increased step-by-step to 100% since December 2007.

c HIRDLS

The High Resolution Dynamics Limb Sounder (HIRDLS, see Appendix A) is one of the instruments on the Aura spacecraft, which was launched into a near polar, sun-synchronous orbit with a period of approximately 100 min. HIRDLS is a multi-channel, infrared radiometer designed to measure radiated thermal emissions from the atmospheric limb at various spectral intervals in the range 6–17 μm , chosen to correspond to specific gases and atmospheric “windows”. The final output is a set of global 3-D fields of atmospheric temperature, several minor constituents and geostrophic winds. The instrument provides measurements of temperature, trace constituents and aerosols from the middle troposphere to the mesosphere, with a key attribute of high vertical resolution. HIRDLS also yields measurements of atmospheric aerosols and cirrus clouds, as well as unique measurements of sub-visible cirrus.

After launch, activation of the HIRDLS instrument revealed that the optical path was blocked so that only 20% of the aperture could view the Earth’s atmosphere. Engineering studies suggest that a piece of thermal blanketing material ruptured from the back of the instrument during the explosive decompression of launch. Attempts to remove this material failed. However, even with the 80% blockage, measurements at high vertical resolution can be made at one scan angle. An example of HIRDLS measurements is provided in Fig. 3.9. The HIRDLS chopper stopped on 17th March 2008 and attempts to restart it have been unsuccessful.

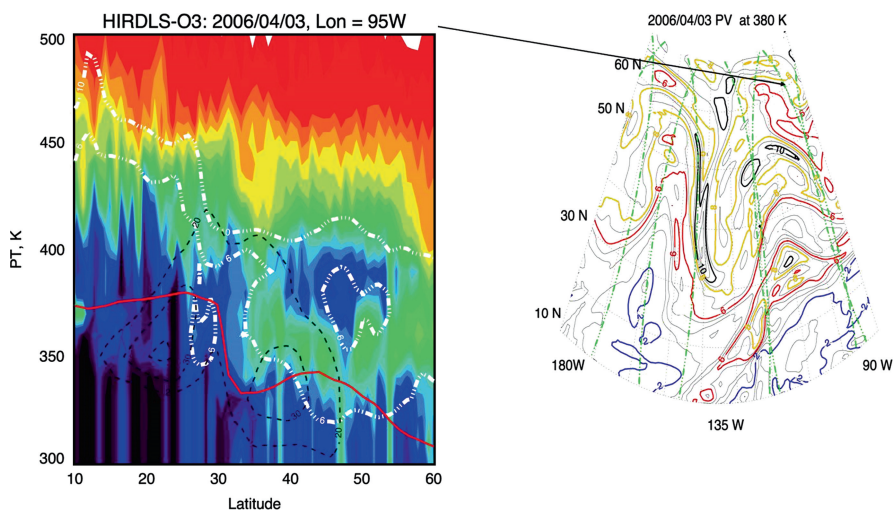


Fig. 3.9 Ozone tropospheric intrusion event as detected from HIRDLS/ Aura on 2nd, 3rd and 4th April 2006 (Courtesy to the HIRDLS Science team, available from <http://www.eos.ucar.edu/hirdls/>).

3.4.2 Nadir Looking Instruments

a IMG

As mentioned in Section 3.2.2, IMG/ADEOS (see Appendix A) used a nadir-viewing Fourier transform interferometer that recorded the thermal emission of the Earth-atmosphere system between 600 and 3,030 cm^{-1} , with a maximum optical path difference of 10 cm (i.e. 0.1 cm^{-1} unapodized spectral resolution) to sound the atmosphere (Kobayashi et al. 1999).

ADEOS was a sun-synchronous (equator local crossing time at descending node at 10:30 a.m.), ground track repeat, polar-orbiting satellite. The instrument performed a global coverage of the Earth, making 14 1/4 orbits per day with a series of six successive measurements separated by 86 km (every 10 s) along the track. The footprint on the ground was 8×8 km, in three spectral bands, corresponding to three different detectors and three geographically adjacent footprints. Due to the large data rate, the operational mode of IMG was set to 4 days operation/10 days halt alternation, except for one specific period from 1st–10th April 1997 for which 10 consecutive days were available.

b MOPITT

The MOPITT instrument (see Appendix A), Measurements Of Pollution In The Troposphere, is a correlation radiometer instrument with channels at around 4.7 μm and 2.2 μm . The original mission was targeted at CO and CH_4 , but only CO measurements have been produced. However the mission, launched in December 1999 has produced, at the time of writing, a ten year record of CO over the planet. MOPITT has a 22×22 km pixel and a scanning swath of ~650 km (29 pixels). It produces continuous coverage within that swath as the satellite flies in a sun-synchronous orbit at 705 km and 98.4° inclination. The planet is mostly covered in about 4 days and the ground coverage has a 16-day repeat cycle. A typical plot of MOPITT L2 “total column” amount of CO over the globe is shown in Fig. 3.10. It is a composite of data taken between 28th November and 6th August 2000 gridded to $1^\circ \times 1^\circ$. The gaps in the data are mainly the result of persistent cloud cover in those regions. Biomass burning events in South America and Africa can clearly be seen and a plume of CO extends around the planet eventually fetching up against the Andes.

The MOPITT data products released are from the CO 4.7 μm channels and represent vertical profiles of CO mixing ratios. On the global and seasonal scales the climatology of the CO distribution has been obtained using MOPITT CO data depicting major sources of CO emission on the planet (Edwards et al. 2004; 2006a). Edwards et al. (2006b) showed also that inter-annual components of the CO variation over marine continents and northern Australia are well correlated with El Niño events because dry conditions favour forest fires. On the synoptic scale

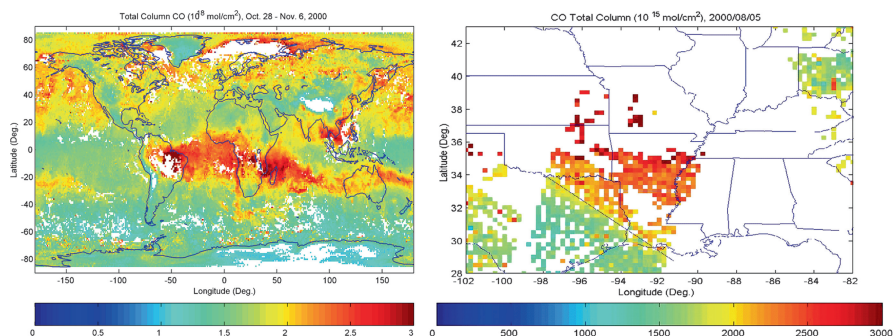


Fig. 3.10 *Left*: Global distribution of MOPITT L2 CO total column amount (8 months average). *Right*: frontal system over Texas on 5th August 2000. (Liu et al. 2006).

large horizontal gradients of CO identified in the MOPITT data have been associated with vertical and horizontal transport of air with different CO concentrations under distinctive meteorological conditions (Liu et al. 2006). Fig. 3.10 shows a frontal system over Texas in May 2000. The transition from a relatively polluted air mass to the south and the cleaner mass to the north is easily seen. The capability of observing vertical structure of tropospheric CO by MOPITT has been demonstrated in a number of papers. There were examples of strong enhancement of upper tropospheric CO in the Asian summer monsoon region due to deep convective transport (Kar et al. 2004), and enhanced CO over the Zagros mountains in Iran generated in a process of mountain venting (Kar et al. 2006). MOPITT data have also been used to isolate plumes of CO in several cities and urban areas where the CO emissions are mainly anthropological (Clerbaux et al. 2008a). A recent study using MOPITT 2.3 μm channels has reported encouraging results in the retrieval of the CO total column in reflected sunlight (Deeter et al. 2009).

c AIRS

Launched into Earth-orbit in May 2002, the Atmospheric Infrared Sounder, AIRS is one of six instruments on board the Aqua satellite, part of the NASA Earth Observing System (see Appendix A). It observes the global water and energy cycles, climate variation and trends, and the response of the climate system to increased greenhouse gases.

AIRS is designed to create three dimensional maps of air and surface temperature, water vapour, and cloud properties. AIRS has 2378 spectral channels in the range 3.74–15.4 μm and good spectral resolution ($\lambda/\Delta\lambda \sim 1,200$). It provides accurate information on the vertical profiles of atmospheric temperature and moisture. AIRS can also measure trace greenhouse gases such as O_3 , CO, and to some extent CO_2 (see Fig. 3.11), and CH_4 .

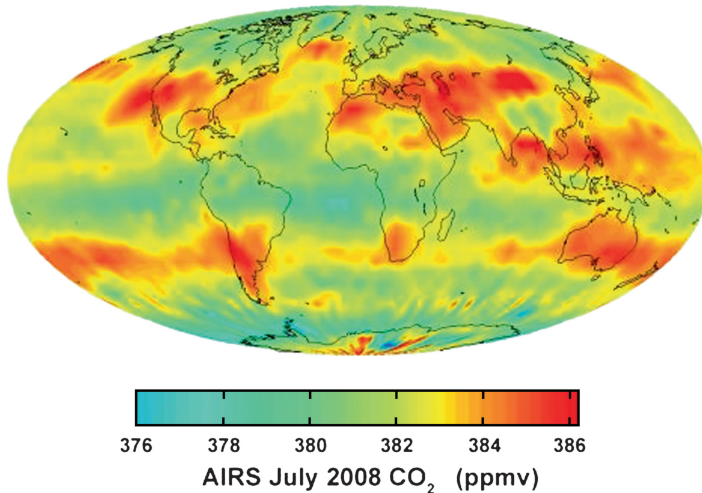


Fig. 3.11 An image created with data acquired by AIRS during July 2008. It shows large scale patterns of CO₂ concentrations that are transported around the Earth by the general circulation of the atmosphere. The effect of the northern hemisphere mid-latitude jet stream is to set the northern limit of enhanced CO₂. The zonal flow of the southern hemisphere mid-latitude jet stream results in a belt of enhanced CO₂ girdling the globe, fed by biogenesis activity in South America, forest fires in both South America and central Africa, the clusters of gasification plants in South Africa and power generation in southeastern Australia. (Image courtesy of NASA/JPL, <http://www.nasa.gov/topics/earth/features/airs-20081009.html>).

d TES

The Tropospheric Emission Spectrometer (TES, see Appendix A) was launched on the Aura satellite in July 2004 into a sun-synchronous orbit with an equator crossing time of 13:43. TES is a FTS with a resolution of 0.015 cm^{-1} (minimum, unapodized) and a spectral range of $650\text{--}2,250 \text{ cm}^{-1}$ in a number of bands. It is designed to operate in both limb viewing and nadir viewing modes, although most data have been collected in the nadir viewing mode with a resolution of 0.06 cm^{-1} (unapodized). The entire instrument is cooled with a set of active coolers. The detectors consist of 16×1 arrays aligned along the direction of motion in nadir mode and vertically in limb mode. The 16 pixels on the ground in nadir view an area of $26 \times 42 \text{ km}^2$. The instrument is capable of measuring a large range of molecules including O₃, CO, CO₂, CH₄, NO, N₂O, NO₂, SO₂, NH₃, HNO₃, CFCs etc. The instrument is also capable of making measurements in a number of modes that offer different combinations of coverage and measurement density including a “global survey” mode consisting of measurements about 5° apart along the orbit track and a step/stare mode that increases the measurement density to $\sim 0.4^\circ$ apart or about 6 s between observations.

The cooled spectrometer has a sufficient signal to noise ratio and spectral resolution to allow the separation of the tropospheric component of gases from the stratospheric component and also to provide some vertical resolution of the concentrations. It has thus been possible to measure tropospheric ozone directly (Jourdain et al. 2007) with some vertical resolution, as shown in Fig. 3.12. In addition it has been possible to detect and measure isotopes of water (Worden et al. 2007b) and also very low concentrations of gases such as NH_3 and CH_3OH (Beer et al. 2008). For several of these measurements the step/stare observing mode was used to enhance the geographical coverage.

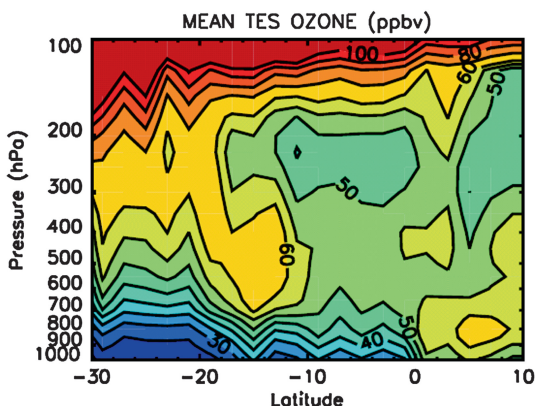


Fig. 3.12 Cross-section of O_3 mixing ratios in ppbv for longitudes over the tropical Atlantic Ocean for 22nd to 25th January 2005. DOFS for the troposphere for these measurements is ~ 1.5 (Jourdain et al. 2007).

e IASI

IASI, the Infrared Atmospheric Sounding Interferometer (see Appendix A), is a series of tropospheric remote sensors to be carried for a period of 14 years on the Metop-A, B, and C weather satellites deployed as part of the European Polar System which started in 2006. It is a joint undertaking of the French Space agency CNES (Centre National d'Etudes Spatiales) and EUMETSAT, the European organization for the exploitation of meteorological satellites, with CNES managing the instrumental development part and EUMETSAT operating the instrument in orbit.

The instrument comprises a FTS and an imaging system, designed to measure the infrared spectrum emitted by the Earth in the thermal infrared using a nadir geometry. The instrument provides spectra of high radiometric quality at 0.5 cm^{-1} spectral resolution, from 645 to $2,760 \text{ cm}^{-1}$. IASI has a square field of view sampled by a matrix of 2×2 circular pixels of 12 km each and is providing measurements each 25 km at nadir with a good horizontal coverage due to its ability to scan across track with a swath width of $\pm 1,026 \text{ km}$.

IASI provides improved infrared soundings of the temperature profiles in the troposphere and lower stratosphere, moisture profiles in the troposphere, as well as some of the chemical components playing a key role in climate monitoring, global change and atmospheric chemistry (Clerbaux et al. 2009). From the geophysical products that can be derived from the IASI spectra four classes of compounds can be distinguished (see Fig. 3.6):

1. Absorbers with long lifetimes (>50 years) and stable atmospheric concentrations, which require accurate retrievals in order to provide useful information on their global or temporal variability (accuracy lower than a few percent is required). These are principally the strongly absorbing climate gases, namely, CO_2 (Crevoisier et al. 2009a) and N_2O (Ricaud et al. 2009). The retrieval of their concentration from IASI observations requires specific methods and averaging over time and/or space. CFC-11, CFC-12 and HCFC-22, the most abundant substitute of chlorofluorocarbons, are also detectable. Additionally the long-lived OCS is identified in the spectra (Shephard et al. 2009).
2. Strong to medium absorbers which exhibit a significant atmospheric variability ($>5\%$) because of their reactivity (lifetimes from a few weeks to a few years), which can be observed in each individual IASI observation. These species, which contribute to tropospheric and/or stratospheric chemistry, are water vapour (H_2O and isotopologues HDO and H_2^{18}O) (Herbin et al. 2009), CH_4 (Crevoisier et al. 2009b; Razavi et al. 2009), O_3 (Eremenko et al. 2008; Boynard et al. 2009; Keim et al. 2009), CO (George et al. 2009; Turquety et al. 2009; Fortems-Cheinet et al. 2009) and HNO_3 (Wespes et al. 2009).
3. Weak absorbers that can only be detected above emission sources or in concentrated plumes owing to the good radiometric performance of IASI. These include SO_2 from volcanoes (Clarisse et al. 2008), see Fig. 3.13, NH_3 from biomass burning and intensive land use (Clarisse et al. 2009) and volatile organic compounds such as HCOOH , CH_3OH , C_2H_4 and PAN (peroxyacetyl nitrate) from biomass burning (Coheur et al. 2009).
4. Higher altitude aerosols, such as those resulting from sandstorms, volcanic eruptions or cirrus formation. They mainly manifest themselves in the $700\text{--}1,300\text{ cm}^{-1}$ window as broad absorption features.

3.5 Future Plans for Tropospheric Sounders

Retrieval development has been very rapid and is probably approaching the limits of the information contained in the signals detected. Improvements can be seen in vertical resolution and in error treatments and these will benefit from higher performance instrumentation. More complex, or “global” retrievals, whether of multiple species, locations or times, will be used more as computational techniques and computer power improve. Finally, data assimilation and the use of models in retrievals will probably become more routine. These techniques currently

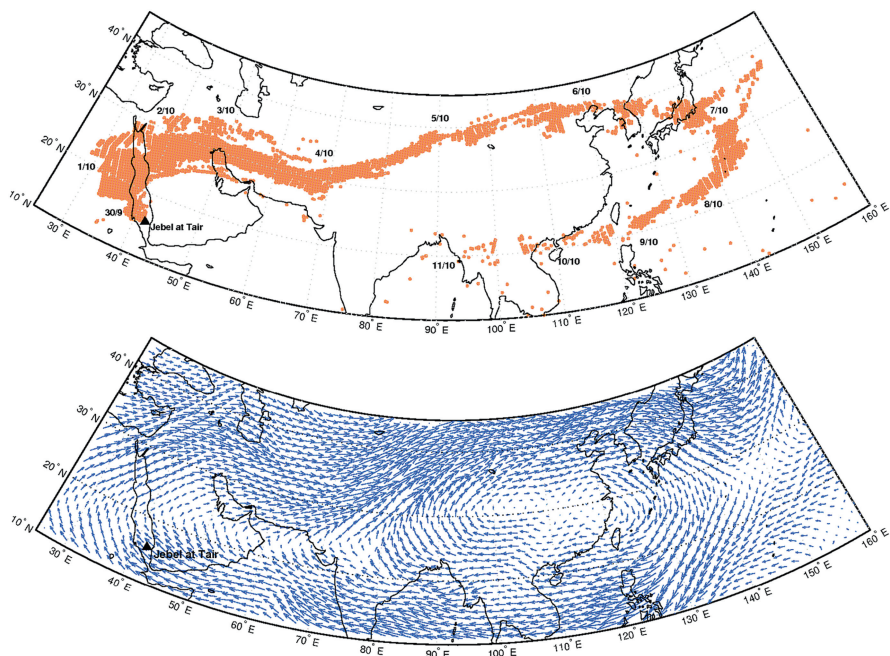


Fig. 3.13 Top: Integrated view of SO_2 as measured by IASI after the Jebel al Tair (Red Sea) eruption, on 30th September 2007. Bottom: ECMWF winds at 100 hPa (Clarisse et al. 2008).

assimilate profile data (level 2 data), but in the near future will switch to the assimilation of radiances (level 1 data) or, in some cases, raw instrument output (level 0 data).

As the population of the planet continues to increase, and with it the industrial activity, the importance of protecting air quality increases. The potential for harm and the consequences become steadily more serious. Thus the forecasting of chemical weather is likely to become main-stream in the next decade and this will require considerable efforts in both the modelling and instrumentation areas to produce timely and accurate forecasts of conditions around major population centres. Already many nations and supra-national organizations are regulating air quality, and compliance with the regulations becomes a significant societal and economic issue.

In the future, infrared remote sounding of the atmosphere will continue to develop. There are strong drivers from the scientific and regulatory areas for higher temporal coverage while maintaining good spatial coverage. There is also the transition from research instrumentation to operational instruments.

All the instruments launched so far have been on polar orbiting satellites (with the major exception of shuttle and shuttle-launched instrumentation). The majority of these satellites have also been sun synchronous. However the time resolution of these instruments is at best two measurements per location per day, and frequently lower.

In order to increase the spatial sampling, two approaches are possible: satellite arrays and higher orbits. Satellite arrays are technologically possible, requiring nothing more than duplication of equipment, costs will need to be examined, but the major issue will become cross-calibration of the array since all of these instruments are extremely sensitive to small changes in the local spacecraft environment. The most frequently discussed higher orbit is the geosynchronous/geostationary orbit which permits continuous measurements over about 25% of the globe from any one satellite. In this configuration hourly measurements at equatorial and mid-latitudes are a possibility. However in order to capture the major populated and industrial areas of the planet, at least three satellites are required and perhaps, more realistically, four. Plans to launch thermal infrared instruments on a geostationary orbit are progressing and are now at different maturity levels in the EU, USA and in Asia¹.

The polar regions are inaccessible from a geostationary orbit but well served by the instrumentation on LEO platforms. In order to measure at high latitudes either polar orbiting satellites will be required or perhaps a more exotic orbit such as the Molniya orbit, but for air quality sensing alone the costs may be prohibitive. There is however a strong motivation for such measurements as the solar zenith angle at the poles is always large and the shorter-wavelength techniques that rely on reflected solar energy are less effective. Thus longer wavelength infrared techniques become essential.

On the technological front, detector performance and array size can continue to grow, the former only modestly because of the fundamental limits of physics: when the quantum efficiency of the detection process approaches unity and one electron is produced for each photon input and so there is no further room for improvement. Array size can continue to increase and cooling requirements can be reduced through detectors that operate at higher temperatures and reduced thermal leakage in the structure. Spectral resolution can be raised in concert with higher performance detectors and more efficient optics.

It is worth noting that there are surprisingly few atmospheric chemistry missions projected for the future, both in the nadir and limb/occultation geometry, compared to those available now.

References

- Beer, R., Shephard, M.W., Kulawik, S.S., Clough, S.A., Eldering, A., Bowman, K.W., Sander, S.P., Fisher, B.M., Payne, V.H., Luo, M., Osterman, G.B., and Worden, J.R., 2008, First satellite observations of lower tropospheric ammonia and methanol. *Geophys. Res. Lett.* doi:10.1029/2008GL033642.

¹For US plans see NASA's NFS decadal study (<http://decadal.gsfc.nasa.gov/missions.html>)

For EU plans see the Eumetsat MTG satellite concept (http://www.eumetsat.int/Home/Main/What_We_Do/Satellites/Future_Satellites/)

- Bernath, P.F., McElroy, C.T., Abrams, M.C., Boone, C.D., Butler, M., Camy-Peyret, C., Carleer, M., Clerbaux, C., Coheur, P.F., Colin, R., DeCola, P., Maziere, M.D., Drummond, J.R., Dufour, D., Evans, W.F.J., Fast, H., Fussen, D., Gilbert, K., Jennings, D.E., Llewellyn, E. J., Lowe, R.P., Mahieu, E., McConnell, J.C., McHugh, M., McLeod, S.D., Michaud, R., Midwinter, C., Nassar, R., Nichitiu, F., Nowlan, C., Rinsland, C.P., Rochon, Y.J., Rowlands, N., Semeniuk, K., Simon, P., Skelton, R., Sloan, J.J., Soucy, M.-A., Strong, K., Tremblay, P., Turnbull, D., Walker, K.A., Walkty, I., Wardle, D.A., Wehrle, V., Zander, R., and Zou, J., 2005, Atmospheric Chemistry Experiment (ACE): mission overview. *Geophys. Res. Lett.* doi:10.1029/2005GL022386.
- Bowman, K.W., C.D. Rodgers, S.S. Kulawik, J. Worden, E. Sarkissian, G. Osterman, T. Steck, Ming Lou, A. Eldering, M. Shephard, H. Worden, M. Lampel, S. Clough, P. Brown, C. Rinsland, M. Gunson and R. Beer, 2006, Tropospheric Emission Spectrometer: Retrieval Method and Error Analysis. *IEEE Trans. Geosci. Remote Sens.*, **44**, 1297–1307.
- Boynard, A., C. Clerbaux, P.-F. Coheur, D. Hurtmans, S. Turquety, M. George, J. Hadji-Lazaro, C. Keim and J. Meyer-Arnek, 2009, Measurements of total and tropospheric ozone from IASI: comparison with correlative satellite, ground-based and ozonesonde observations. *Atmos. Chem. Phys.*, **9**, 6255–6271.
- Clarisse, L., P.F. Coheur, A.J. Prata, D. Hurtmans, A. Razavi, T. Phulpin, J. Hadji-Lazaro and C. Clerbaux, 2008, Tracking and quantifying volcanic SO₂ with IASI, the September 2007 eruption at Jebel at Tair. *Atmos. Chem. Phys.*, **8**, 7723–7734.
- Clarisse, L., Clerbaux, C., Dentener, F., Hurtmans, D., and Coheur, P.-F., 2009, Global ammonia distribution derived from infrared satellite observations. *Nature Geoscience*, doi:10.1038/ngeo551.
- Clerbaux, C., J. Hadji-Lazaro, S. Turquety, G. Mégie and P.-F. Coheur, 2003, Trace gas measurements from infrared satellite for chemistry and climate applications. *Atmos. Chem. Phys.*, **3**, 1495–1508.
- Clerbaux, C., Edwards, D.P., Deeter, M., Emmons, L., Lamarque, J-F., Tie, X.X., Massie, S.T., and Gille, J., 2008a, Carbon monoxide pollution from cities and urban areas observed by the Terra/MOPITT mission. *Geophys. Res. Lett.* doi:10.1029/2007GL032300.
- Clerbaux, C., M. George, S. Turquety, K.A. Walker, B. Barret, P. Bernath, C. Boone, T. Borsdorff, J.P. Cammas, V. Catoire, M. Coffey, P.-F. Coheur, M. Deeter, M. De Mazière, J. Drummond, P. Duchatelet, E. Dupuy, R. de Zafra, F. Eddounia, D.P. Edwards, L. Emmons, B. Funke, J. Gille, D.W.T. Griffith, J. Hannigan, F. Hase, M. Höpfner, N. Jones, A. Kagawa, Y. Kasai, I. Kramer, E. Le Flochmoën, N.J. Livesey, M. López-Puertas, M. Luo, E. Mahieu, D. Murtagh, P. Nédélec, A. Pazmino, H. Pumphrey, P. Ricaud, C.P. Rinsland, C. Robert, M. Schneider, C. Senten, G. Stiller, A. Strandberg, K. Strong, R. Sussmann, V. Thouret, J. Urban and A. Wiacek, 2008b, CO measurements from the ACE-FTS satellite instrument: data analysis and validation using ground-based, airborne and spaceborne observations. *Atmos. Chem. Phys.*, **8**, 2569–2594.
- Clerbaux, C., A. Boynard, L. Clarisse, M. George, J. Hadji-Lazaro, H. Herbin, D. Hurtmans, M. Pommier, A. Razavi, S. Turquety, C. Wespes and P.-F. Coheur, 2009, Monitoring of atmospheric composition using the thermal infrared IASI/MetOp sounder. *Atmos. Chem. Phys.*, **9**, 6041–6054.
- Coheur, P.-F., H. Herbin, C. Clerbaux, D. Hurtmans, W. Wespes, M. Carleer, S. Turquety, C.P. Rinsland, J. Remedios, D. Hauglustaine, C.D. Boone and P.F. Bernath, 2007, ACE-FTS observation of a young biomass burning plume: first reported measurements of C₂H₄, C₃H₆O, H₂CO and PAN by infrared occultation from space. *Atmos. Chem. Phys.*, **7**, 5437–5446.
- Coheur, P.-F., L. Clarisse, S. Turquety, D. Hurtmans and C. Clerbaux, 2009, IASI measurements of reactive trace species in biomass burning plumes. *Atmos. Chem. Phys.*, **9**, 5655–5667.
- Crevoisier, C., A. Chédin, H. Matsueda, T. Machida, R. Armante and N. A. Scott, 2009a, First year of upper tropospheric integrated content of CO₂ from IASI hyperspectral infrared observations. *Atmos. Chem. Phys.*, **9**, 4797–4810.

- Crevoisier, C., D. Nobileau, A. M. Fiore, R. Armante, A. Chédin and N. A. Scott, 2009b, Tropospheric methane in the tropics – first year from IASI hyperspectral infrared observations. *Atmos. Chem. Phys.*, **9**, 6337–6350.
- Deeter, M.N., Edwards, D.P., Gille, J.C., and Drummond, J.R., 2009, CO retrievals based on MOPITT near-infrared observations. *J. Geophys. Res.* doi:10.1029/2008JD010872.
- Doicu, A., Schreier, F., and Hess, M., 2004, Iterative regularization methods for atmospheric remote sensing. *J. Quant. Spectrosc. Radiat. Transfer.* doi:10.1016/S0022-4073(02)00292-3.
- Dufour, G., S. Szopa, D.A. Hauglustaine, C.D. Boone, C.P. Rinsland and P.F. Bernath, 2007, The influence of biogenic emissions on upper-tropospheric methanol as revealed from space. *Atmos. Chem. Phys.*, **7**, 6119–6129.
- Edwards, D.P., Emmons, L.K., Hauglustaine, D.A., Chu, A., Gille, J.C., Kaufman, Y.J., Petron, G., Yurganov, L.N., Giglio, L., Deeter, M.N., Yudin, V., Ziskin, D.C., Warner, J., Lamarque, D.F., Francis, G.L., Ho, S.P., Mao, D., Chen, J., Grechko, E.I., and Drummond, J. R., 2004, Observations of Carbon Monoxide and Aerosol From the Terra Satellite: Northern Hemisphere Variability. *J. Geophys. Res.* doi:10.1029/2004JD0047272004.
- Edwards, D.P., Pétron, G., Novelli, P.C., Emmons, L.K., Gille, J.C., and Drummond, J.R., 2006a, Southern Hemisphere carbon monoxide interannual variability observed by Terra/Measurement of Pollution in the Troposphere (MOPITT). *J. Geophys. Res.* doi:10.1029/2006JD007079.
- Edwards, D.P., Emmons, L.K., Gille, J.C., Chu, A., Attie, J.-L., Giglio, L., Wood, S.W., Haywood, J., Deeter, M.N., Massie, S.T., Ziskin, D.C., and Drummond, J. R., 2006b, Satellite-observed pollution from Southern Hemisphere biomass burning. *J. Geophys. Res.* doi:10.1029/2005JD006655.
- Eremenko, M., Dufour, G., Foret, G., Keim, C., Orphal, J., Beekmann, M., Bergametti, G., and Flaud, J.-M., 2008, Tropospheric ozone distributions over Europe during the heat wave in July 2007 observed from infrared Nadir spectra measured by IASI. *Geophys. Res. Lett.* doi:10.1029/2008GL034803.
- Fischer, H., M. Birk, C. Blom, B. Carli, M. Carlotti, T. von Clarmann, L. Delbouille, A. Dudhia, D. Ehhalt, M. Endemann, J.M. Flaud, R. Gessner, A. Kleinert, R. Koopmann, J. Langen, M. López-Puertas, P. Mosner, H. Nett, H. Oelhaf, G. Perron, J. Remedios, M. Ridolfi, G. Stiller and R. Zander, 2008, MIPAS: an instrument for atmospheric and climate research. *Atmos. Chem. Phys.*, **8**, 2151–2188.
- Flaud, J.-M. and H. Oelhaf, 2004, Infrared spectroscopy and the terrestrial atmosphere. *C. R. Physique* **5**, 259–271.
- Fortems-Cheinet, A., F. Chevallier, I. Pison, P. Bousquet, C. Carouge, C. Clerbaux, P.F. Coheur, M. George, D. Hurtmans and S. Szopa, 2009, On the capability of IASI measurements to inform about CO surface emissions. *Atmos. Chem. Phys. Discuss.*, **9**, 7505–7529.
- George, M., C. Clerbaux, D. Hurtmans, S. Turquety, P.-F. Coheur, M. Pommier, J. Hadji-Lazaro, D.P. Edwards, H. Worden, M. Luo, C. Rinsland and W. McMillan, 2009, Carbon monoxide distributions from the IASI/METOP mission: evaluation with other space-borne remote sensors. *Atmos. Chem. Phys. Discuss.*, **9**, 9793–9822.
- Gunson, M.R., M.M. Abbas, M.C. Abrams, M. Allen, L.R. Brown, T.L. Brown, A.Y. Chang, A. Goldman, F.W. Irion, L.L. Lowes, E. Mahieu, G.L. Manney, H.A. Michelsen, M.J. Newchurch, C.P. Rinsland, R.J. Salawitch, G.P. Stiller, G.C. Toon, Y.L. Yung and R. Zander, 1996, The Atmospheric Trace Molecule Spectroscopy (ATMOS) experiment: Deployment on the ATLAS Space Shuttle missions. *Geophys. Res. Lett.*, **23**, 2333–2336.
- Herbin, H., D. Hurtmans, C. Clerbaux, L. Clarisse and P.-F. Coheur, 2009, H₂¹⁶O and HDO measurements with IASI/MetOp. *Atmos. Chem. Phys. Discuss.*, **9**, 9267–9290.
- Jacquinet-Husson, N., Scott, N.A., Chédin, A., Crépeau, L., Armante, R., Capelle, V., Orphal, J., Coustenis, A., Boone, C., Poulet-Crovisier, N., Barbe, A., Birk, M., Brown, L.R., Camy-Peyret, C., Claveau, C., Chance, K., Christidis, N., Clerbaux, C., Coheur, P.F., Dana, V., Daumont, L., De Backer-Barilly, M.R., Di Lonardo, G., Flaud, J.M., Goldman, A., Hamdouni, A., Hess, M., Hurley, M.D., Jacquemart, D., Kleiner, I., Köpke, P., Mandin, J.Y., Massie, S.,

- Mikhailenko, S., Nemtchinov, V., Nikitin, A., Newnham, D., Perrin, A., Perevalov, V.I., Pinnock, S., Régalia-Jarlot, L., Rinsland, C. P., Rublev, A., Schreier, F., Schult, L., Smith, K.M., Tashkun, S.A., Teffo, J.L., Toth, R.A., Tyuterev, V.I.G., Vander Auwera, J., Varanasi, P., Wagner, G., 2008, The GEISA spectroscopic database: Current and future archive for Earth and Planetary atmosphere studies. *J. Quant. Spectrosc. Rad. Transfer.* doi:10.1016/j.jqsrt.2007.12.015.
- Jourdain, L., Worden, H.M., Worden, J.R., Bowman, K, Li, Q., Eldering, A., Kulawik, S.S., Osterman, G., Boersma, K.F., Fisher, B., Rinsland, C.P., Beer, R., and Gunson, M., 2007, Tropospheric vertical distribution of tropical Atlantic ozone observed by TES during the northern African biomass burning season. *Geophys. Res. Lett.* doi:10.1029/2006GL028284.
- Kar, J., Bremer, H., Drummond, J.R., Rochon, Y.J., Jones, D.B.A., Nichitiu, F., Zou, J., Liu, J., Gille, J.C., Edwards, D.P., Deeter, M.N., Francis, G., Ziskin, D., and Warner, J., 2004, Evidence of Vertical Transport of Carbon Monoxide From Measurements of Pollution in the Troposphere (MOPITT). *Geophys. Res. Lett.* doi:10.1029/2004GL021128.
- Kar, J., Drummond, J.R., Jones, D.B.A., Liu, J., Nichitiu, F., Zou, J., Gille, J.C., Edwards, D.P., and Deeter, M.N., 2006, Carbon monoxide (CO) maximum over the Zagros mountains in the Middle East: Signature of mountain venting? *Geophys. Res. Lett.* doi:10.1029/2006GL026231.
- Keim, C., G.Y. Liu, C.E. Blom, H. Fischer, T. Gulde, M. Höpfner, C. Piesch, F. Ravegnani, A. Roiger, H. Schlager and N. Sitnikov, 2008, Vertical profile of peroxyacetyl nitrate (PAN) from MIPAS-STR measurements over Brazil in February 2005 and its contribution to tropical UT NO_y partitioning. *Atmos. Chem. Phys.*, **8**, 4891–4902.
- Keim, C., M. Eremenko, J. Orphal, G. Dufour, J.-M. Flaud, M. Höpfner, A. Boynard, C. Clerbaux, S. Payan, P.-F. Coheur, D. Hurtmans, H. Claude, H. Dier, B. Johnson, H. Kelder, R. Kivi, T. Koide, M. López Bartolomé, K. Lambkin, D. Moore, F. J. Schmidlin and R. Stübi, 2009, Tropospheric ozone from IASI: comparison of different inversion algorithms and validation with ozone sondes in the northern middle latitudes. *Atmos. Chem. Phys. Discuss.*, **9**, 11441–11479.
- Kleinert, A., G. Aubertin, G. Perron, M. Birk, G. Wagner, F. Hase, H. Nett and R. Poulin, 2007, MIPAS Level 1B algorithms overview: operational processing and characterization. *Atmos. Chem. Phys.*, **7**, 1395–1406.
- Kobayashi, H., A. Shimota, C. Yoshigahara, I. Yoshida, Y. Uehara and K. Kondo, Satellite-borne high-resolution FTIR for lower atmosphere sounding and its evaluation. *IEEE Trans. Geosci. Remote Sens.*, **37**, 1496–1507, 1999.
- Kulawik, S.S., G. Osterman and D. Jones, 2006, Calculation of altitude-dependent Tikhonov constraints for TES nadir retrievals. *IEEE Trans. Geosci. Remote Sens.*, **44**, 1334–1342.
- Liu, J., Drummond, J.R., Jones, D.B.A., Cao, Z., Bremer, H., Kar, J., Zou, J., Nichitiu, F., and Gille, J.C., 2006, Large horizontal gradients in atmospheric CO at the synoptic scale as seen by spaceborne Measurements of Pollution in the Troposphere. *J. Geophys. Res.* doi:10.1029/2005JD006076.
- McCartney, E.J., 1983, Absorption and Emission by Atmospheric Gases: The Physical Processes. J. Wiley & Sons, New York.
- Orphal, J., G. Bergametti, B. Beghin, J.-P. Hebert, T. Steck and J.-M. Flaud, 2005, Monitoring tropospheric pollution using infrared spectroscopy from geostationary orbit. *C. R. Physique*, **6**, 888–896.
- Phillips, C., 2003, A technique for the numerical solution of certain integral equations of the first kind. *J. Assoc. Comput. Math.*, **9**, 84–97.
- Razavi, A., C. Clerbaux, C. Wespes, L. Clarisse, D. Hurtmans, S. Payan, C. Camy-Peyret and P. F. Coheur, 2009, Characterization of methane retrievals from the IASI space-borne sounder. *Atmos. Chem. Phys. Discuss.*, **9**, 7615–7643.
- Reichle, H.G., B.E. Anderson, V. Connors, T.C. Denkins, D.A. Forbes, B.B. Gormsen, R.L. Langenfelds, D.O. Neil, S.R. Nolf, P.C. Novelli, N.S. Pougatchev, M.M. Roell and L.P. Steele, 1999, Space shuttle based global CO measurements during April and October 1994, MAPS instrument, data reduction, and data validation, *J. Geophys. Res.*, **104**(17), 21,443–21,454.

- Ricaud, P., J.-L. Attié, H. Teyssèdre, L. El Amraoui, V.-H. Peuch, M. Matricardi and P. Schluesel, 2009, Equatorial total column of nitrous oxide as measured by IASI on MetOp-A: implications for transport processes. *Atmos. Chem. Phys.*, **9**, 3947–3956.
- Rinsland, C.P., Boone, C.D., Bernath, P.F., Mahieu, E., Zander, R., Dufour, G., Clerbaux, C., Turquety, S., Chiou, L., McConnell, J.C., Neary, L., and Kaminski, J.W., 2006, First space-based observations of formic acid (HCOOH): Atmospheric Chemistry Experiment austral spring 2004 and 2005 Southern Hemisphere tropical-mid-latitude upper tropospheric measurements. *Geophys. Res. Lett.* doi:10.1029/2006GL027128.
- Rothman, L. S., Jacquemart, D., Barbe, A., Chris Benner, D., Birk, M., Brown, L.R., Carleer, M. R., Chackerian, C., Chance, K., Coudert, L.H., Dana, V., Devi, V.M., Flaud, J.-M., Gamache, R.R., Goldman, A., Hartmann, J.-M., Jucks, K.W., Maki, A.G., Mandin, J.-Y., Massie, S.T., Orphal, J., Perrin, A., Rinsland, C.P., Smith, M.A.H., Tennyson, J., Tolchenov, R.N., Toth, R. A., Vander Auwera, J., Varanasi, P., and Wagner, G., 2005, The HITRAN 2004 molecular spectroscopic database. *J. Quant. Spectrosc. Rad. Transfer* doi:10.1016/j.jqsrt.2004.10.008.
- Rothman, L.S., Gordon, I.E., Barbe, A., Benner, D. Chris, Bernath, P.F., Birk, M., Boudon, V., Brown, L.R., Campargue, A., Champion, J.-P., Chance, K., Coudert, L.H., Dana, V., Devi, V.M., Fally, S., Flaud, J.-M., Gamache, R.R., Goldman, A., Jacquemart, D., Kleiner, I., Lacome, N., Lafferty, W.J., Mandin, J.-Y., Massie, S.T., Mikhailenko, S. N., Miller, C.E., Moazzen-Ahmadi, N., Naumenko, O.V., Nikitin, A.V., Orphal, J., Perevalov, V.I., Perrin, A., Predoi-Cross, A., Rinsland, C.P., Rotger, M., Šimečková, M., Smith, M.A.H., Sung, K., Tashkun, S.A., Tennyson, J., Toth, R.A., Vandaele, A.C., Vander Auwera, J., 2009, The HITRAN 2008 molecular spectroscopic database. *J. Quant. Spectrosc. Rad. Transfer* doi:10.1016/j.jqsrt.2009.02.013.
- Rodgers, C. D., 1976, Retrieval of atmospheric temperature and composition from remote measurements of thermal radiation. *Rev. Geophys.*, **14**(4), 609–624.
- Rodgers, C.D., 2000, Inverse methods for atmospheric sounding: Theory and Practice. *Atmospheric Oceanic Planet. Phys.*, **2**, World Sci., River Edge, N.J.
- Shephard, M.W., S.A. Clough, V.H. Payne, W.L. Smith, S. Kireev and K.E. Cady-Pereira, 2009, Performance of the line-by-line radiative transfer model (LBLRTM) for temperature and species retrievals: IASI case studies from JAIVEx. *Atmos. Chem. Phys. Discuss.*, **9**, 9313–9366.
- Steck, T., 2002, Methods for determining regularization for atmospheric retrieval problems, *Appl. Opt.*, **41**, 1788–1797.
- Tarantola, A., 2005, Inverse Problem Theory, siam, <http://www.ipgp.jussieu.fr/~tarantola/Files/Professional/Books/InverseProblemTheory.pdf>
- Tikhonov, A., 1963, On the solution of incorrectly stated problems and a method of regularization. *Dokl. Acad. Nauk SSSR*, **151**, 501–504.
- Turquety, S., Hadji-Lazaro, J., Clerbaux, C., Hauglustaine, D.A., Clough, S.A., Cassé, V., Schlüssel, P., and Mégie, G., 2004, Operational trace gas retrieval algorithm for the Infrared Atmospheric Sounding Interferometer. *J. Geophys. Res.* doi:10.1029/2004JD004821.
- Turquety, S., D. Hurtmans, J. Hadji-Lazaro, P.-F. Coheur, C. Clerbaux, D. Josset and C. Tsamalis, 2009, Tracking the emission and transport of pollution from wildfires using the IASI CO retrievals: analysis of the summer 2007 Greek fires. *Atmos. Chem. Phys.*, **9**, 4897–4913.
- Wespes, C., D. Hurtmans, C. Clerbaux, M.L. Santee, R.V. Martin and P.F. Coheur, 2009, Global distributions of nitric acid from IASI/MetOP measurements. *Atmos. Chem. Phys. Discuss.*, **9**, 8035–8069.
- Worden, H.M., Logan, J.A., Worden, J.R., Beer, R., Bowman, K., Clough, S.A., Eldering, A., Fisher, B.M., Gunson, M.R., Herman, R.L., Kulawik, S.S., Lampel, M.C., Luo, M., Megretskaya, I.A., Osterman, G.B., Shephard, M.W., 2007a, Comparisons of Tropospheric Emission Spectrometer (TES) ozone profiles to ozonesondes: Methods and initial results. *J. Geophys. Res.* doi:10.1029/2006JD007258.
- Worden, J., Noone, D., Bowman, K., Beer, R., Eldering, A., Fisher, B., Gunson, M., Goldman, A., Herman, R., Kulawik, S.S., Lampel, M., Osterman, G., Rinsland, C., Rodgers, C., Sander, S., Shephard, M., Webster, C.R., and Worden, H., 2007b, Importance of rain evaporation and continental convection in the tropical water cycle. *Nature* doi:10.1038/nature05508.

